The interphase model applied to simulate chemically bonded anchors.

Antonino Spada[1], Giuseppe Fileccia Scimemi[1], Giuseppe Giambanco[1]
[1]*Department of Structural, Aerospace and Geotechnical Engineering, University of Palermo, Italy*
E-mails: antonino.spada@unipa.it, giuseppe.filecciascimemi@unipa.it, ggiamb@unipa.it

Keywords: Contact, interphase, pullout test.

SUMMARY. Epoxy adhesive anchor systems are widely used in civil engineering. They are used to anchor both threaded rods and reinforcing bar into hardened concrete. The pullout test is a standard experimental procedure to evaluate the bond strength between steel/concrete or steel/adhesive/concrete interfaces. The overall response is strongly related to the anisotropy of the structure, and therefore to the mutual static and kinematic relations between the different materials that compose the system. A mesoscale interphase model has been implemented in a research oriented finite element code to simulate experimental tests. In this model the failure can happen both at the contact surfaces (between the joint and bodies interacting with it) and within the same joint. The constitutive laws of the interphase are written in terms of internal state of stress and contact tractions and related kinematic variables.

1 INTRODUCTION

Epoxy adhesive anchor systems are widely used in civil engineering. They are used to bond both threaded rods and reinforcing bars into hardened concrete. For instance, common applications include bridge widening, structure-mounted signs, luminaries and light poles, concrete repair and rehabilitation, and tunneling finishing. In concrete structures chemically bonded anchors are used to cast secondary floor slabs, close temporary openings, cast new wall or expand existing buildings.

Nowadays there is an oncoming wider use of high quality epoxy resins that improve the adhesion between the bonded materials. The use of chemically bonded anchors is sometimes preferred to the cast-in-place method especially in presence of high pullout resistances.

The pullout test is a standard experimental procedure to evaluate the bond strength between steel/concrete or steel/adhesive/concrete interfaces. The overall response is strongly related to the anisotropy of the structure, and therefore to the mutual mechanical and kinematical relations between the different materials that compose it. In pristine conditions the bond between steel and the adhesive, or adhesive and concrete, is due to the chemical adhesion. Chemical adhesion provides the necessary strength to avoid the slipping off of the rebar and, depending on the steel/adhesive/concrete interfaces properties, different failure modes can take place. Different failure modes are discussed in [1]. If the chemical connections fail, relative displacements occur between the two surfaces and, in case of compressive normal stresses or for dilatancy effects, friction forces dominate. In this case the failure mode occurs for frictional sliding.

During the sliding, the mechanical response is affected by what happens on the singularity surfaces. Sliding implies a damaging of the contact surface and as a consequence a diminishing value of tangential stress up to a residual value. Moreover, the kinematical mode mostly depends on the roughness of the contact surfaces, that also induces dilatancy effects.

A possibility to simulate the interface response is to apply a phenomenological constitutive model for which the sliding mode is associated with the interface yield condition expressed in terms of contact tractions and interface state variables whose evolution depends on tangential slip and dilatancy. Another important factor is the microslip effect occurring before the sliding mode takes place at the

contact. Slip and sliding constitute the inelastic behaviour at the fracture surface.

In this paper the pullout behaviour of chemically bonded anchors on concrete cylinders is experimentally and numerically investigated. Experimental pullout tests were conducted on rebars embedded in concrete cylinders by means of polyester resin. A way to simulate the presence of the resin joint is by using interphase elements [2]. The usual assumption used in zero-thickness interface elements where the response is governed by contact stress components, may require a correction by introducing the effect of internal stresses into the analysis. Consequently, in this work a mesoscale interphase model has been implemented in a research oriented finite element code to simulate experimental tests. In this model the failure can happen both on the contact surfaces (between the joint and bodies interacting with it) and within the same joint. The constitutive laws of the interphase are written in terms of internal state of stress and contact tractions and related kinematic variables.

2 THE INTERPHASE MODEL

With the term "Interphase" we refer to a model utilized to represent a material layer able to take into account stresses and strains within and outside the joint. The interface model is substantially an enachement of the "Interface" model (that considers only contact tractions and the relevant displacement jump) so that the response is corrected by adding the contribution of internal state of stresses to the contact ones.

Consider the third body Ω in contact with the two bodies Ω^+ and Ω^- by means of the two physical interfaces Σ^+ and Σ^- respectively, and characterized by d_x an d_y base dimensions and with thickness h as in Fig. 1. The static and kinematics quantities are referred to a Cartesian coordinate system (x, y, z) with x, y axes lying within the middle plane of the joint and the z-axis coinciding with the normal unit vector $\mathbf{n}$ directed towards the body Ω^+. In correspondence with the two physical interfaces Σ^+ and Σ^-, the joint Ω interacts with the two bodies Ω^+ and Ω^- through the following traction components.

$$\mathbf{t}^+ = \left[\begin{array}{ccc} t_x^+ & t_y^+ & t_z^+ \end{array} \right] \quad \text{on} \quad \Sigma^+; \qquad \mathbf{t}^- = \left[\begin{array}{ccc} t_x^- & t_y^- & t_z^- \end{array} \right] \quad \text{on} \quad \Sigma^-,$$

which can be regarded as external surface loads for the joint.

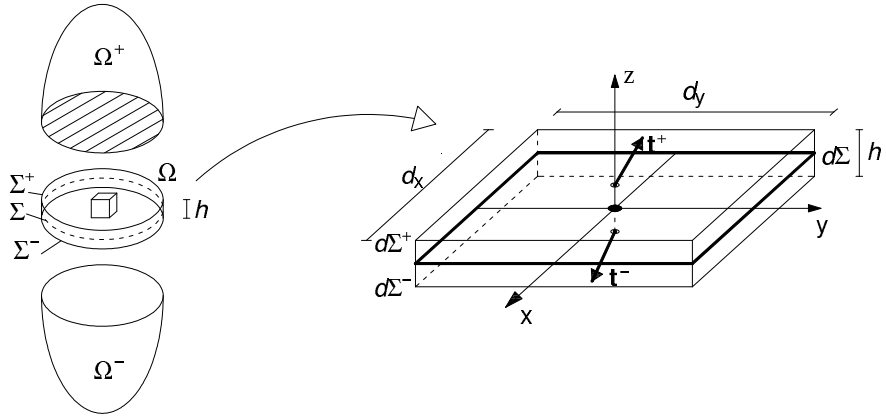

Figure 1: The interphase model.

In order to derive the basic relations of the interphase model, we assume that fibers inside the interphase along the z-direction during the deformation process are maintained rectilinear. Under this assumption the displacement field $\mathbf{u} = \left[\begin{array}{ccc} u_x & u_y & u_z \end{array} \right]$ within the layer can be easily obtained from the displacement fields $\mathbf{u}^+$ and $\mathbf{u}^-$ on the interfaces Σ^+ and Σ^-, thus

$$\mathbf{u}\left(x,y,z\right) = \left(\frac{1}{2} + \frac{z}{h}\right)\mathbf{u}^+\left(x,y\right) + \left(\frac{1}{2} - \frac{z}{h}\right)\mathbf{u}^-\left(x,y\right) \tag{1}$$

where

$$\mathbf{u}^+ = \left[\begin{array}{ccc} u_x^+ & u_y^+ & u_z^+ \end{array} \right] \quad \mathbf{u}^- = \left[\begin{array}{ccc} u_x^- & u_y^- & u_z^- \end{array} \right]$$

The strain tensor inside the joint is derived in a classical way from the displacement field

$$\boldsymbol{\varepsilon} = \nabla^S \mathbf{u} \tag{2}$$

with $\nabla^S = \frac{1}{2}\left(\nabla + \nabla^T\right)$.

Since the thickness of the joint Ω is small if compared to the characteristic dimensions of the elements Ω^+ and Ω^-, we can assume a representative strain state $\hat{\boldsymbol{\varepsilon}}$ constant along the thickness of the joint.

By inserting Eq. 1 into 2, the mean value of $\boldsymbol{\varepsilon}$ along the thickness is given by:

$$\hat{\boldsymbol{\varepsilon}}\left(x,y\right) = \frac{1}{h}\int\limits_{-\frac{h}{2}}^{\frac{h}{2}} \boldsymbol{\varepsilon} dz = \frac{1}{2h}\left[\Delta\mathbf{u}\otimes\mathbf{I}_3 + \left(\Delta\mathbf{u}\otimes\mathbf{I}_3\right)^T\right] + \frac{1}{2}\nabla^S\left(\mathbf{u}^+ + \mathbf{u}^-\right) \tag{3}$$

where $\Delta\mathbf{u} = \mathbf{u}^+ - \mathbf{u}^-$, and $\mathbf{I}_3 = \{\boldsymbol{\delta}_{i3}\}$.

Equilibrium equations are derived by applying the principle of virtual displacements that asserts that the external work produced by the contact tractions must be equal internal work developed in the joint

$$\int\limits_{\Sigma^+} \delta\mathbf{u}^+ \cdot \mathbf{t}^+ d\Sigma^+ + \int\limits_{\Sigma^-} \delta\mathbf{u}^- \cdot \mathbf{t}^- d\Sigma^- = \int\limits_{V} \delta\hat{\boldsymbol{\varepsilon}} : \boldsymbol{\sigma}\, dV \tag{4}$$

In Eq. 4, the independency of $\hat{\boldsymbol{\varepsilon}}$ with respect to z allows to convert the right side integral calculated on the entire volume in an integral expressed on the middle surface Σ by defining a mean value $\hat{\boldsymbol{\sigma}}$ of the stresses along the thickness of the joint.

$$\int\limits_{V} \delta\hat{\boldsymbol{\varepsilon}} : \boldsymbol{\sigma}\, dV = \int\limits_{\Sigma} \delta\hat{\boldsymbol{\varepsilon}} : \hat{\boldsymbol{\sigma}}\, d\Sigma \tag{5}$$

$$\hat{\boldsymbol{\sigma}} = \frac{1}{h}\int\limits_{-\frac{h}{2}}^{\frac{h}{2}} \boldsymbol{\sigma}\, dz \tag{6}$$

If we assume $\Sigma^+ = \Sigma^- = \Sigma$, substituting Eq. 3 into Eq. 4 and by applying the divergence theorem we obtain:

$$\begin{array}{l} \int\limits_{\Sigma} \delta\mathbf{u}^{+T} \left[\mathbf{t}^+ - \hat{\boldsymbol{\sigma}} \cdot \mathbf{I}_3 + \frac{h}{2} div\hat{\boldsymbol{\sigma}}\right] d\Sigma + \int\limits_{\Sigma^-} \delta\mathbf{u}^- \left[\mathbf{t}^- + \hat{\boldsymbol{\sigma}} \cdot \mathbf{I}_3 + \frac{h}{2} div\hat{\boldsymbol{\sigma}}\right] d\Sigma = \\ = \frac{h}{2} \int\limits_{\Gamma} \mathbf{m} \cdot \hat{\boldsymbol{\sigma}} \cdot \left(\delta\mathbf{u}^+ + \delta\mathbf{u}^-\right) d\Gamma \end{array} \tag{7}$$

with $\mathbf{m}$ the normal specifying lateral surface Γ tractions and the perimeter of the joint middle plane Σ.

Since Eq. 7 has to be valid for all the virtual displacements $\delta\mathbf{u}^+$ and $\delta\mathbf{u}^-$, the following equilibrium equations are derived:

$$\mathbf{t}^+ = \hat{\boldsymbol{\sigma}} \cdot \mathbf{I}_3 - \frac{h}{2} div\hat{\boldsymbol{\sigma}} \quad \text{on } \Sigma; \quad \mathbf{t}^- = -\hat{\boldsymbol{\sigma}} \cdot \mathbf{I}_3 - \frac{h}{2} div\hat{\boldsymbol{\sigma}} \quad \text{on } \Sigma, \tag{8}$$

$$\mathbf{m} \cdot \hat{\boldsymbol{\sigma}} = 0 \qquad \text{on } \Gamma. \tag{9}$$

3 THE INTERPHASE FINITE ELEMENT

In this work applications have been developed with regard to 2D problems and in particular plane stress and axisymmetric cases have been faced. The plane stress formulation is here discussed.

The interphase model has been introduced as a new user element in the open-source finite element program FEAP ([3]). The finite element is characterized by 4-node rectangular shaped and two or three Gauss points are used as quadrature rule.

The local reference system is fixed once the vectors $\mathbf{n}$ and $\mathbf{s}$ are known (Fig. 2), and the rotation matrix from the local system to the global one is therefore given by

$$\boldsymbol{\theta} = \left[\begin{array}{cc} \mathbf{s} & \mathbf{n} \end{array}\right] \tag{10}$$

The displacement at each point of the finite element is obtained as a function of the nodal displacements.

If we define the vector $\mathbf{U}$ collecting all the nodal displacements as:

$$\mathbf{U} = \left[\begin{array}{cccccccc} U_{x3} & U_{x4} & U_{x2} & U_{x1} & U_{z3} & U_{z4} & U_{z2} & U_{z1} \end{array}\right]^T, \tag{11}$$

the displacements at each point of the upper or lower boundaries of the interface are therefore given by:

$$\mathbf{u} = \mathbf{N}\,\mathbf{U} \tag{12}$$

where $\mathbf{u} = \left[\begin{array}{cccc} u_x^+ & u_x^- & u_z^+ & u_z^- \end{array}\right]^T$

and $\mathbf{N} = \begin{bmatrix} N_2 & N_1 & 0 & 0 & 0 & 0 & 0 & 0 \\ 0 & 0 & N_2 & N_1 & 0 & 0 & 0 & 0 \\ 0 & 0 & 0 & 0 & N_2 & N_1 & 0 & 0 \\ 0 & 0 & 0 & 0 & 0 & 0 & N_2 & N_1 \end{bmatrix}$.

N_1 and N_2 are the two shape functions given by:

$$N_{1,2}(\xi) = \frac{1}{2}(1 \mp \xi); \quad \xi \in \left[\begin{array}{cc} -1, & 1 \end{array}\right] \tag{13}$$

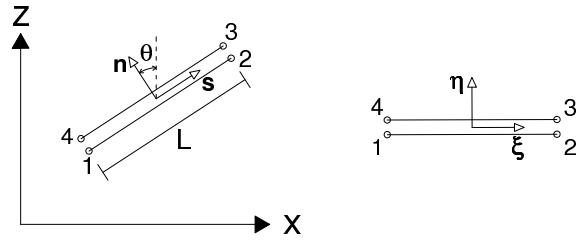

Figure 2: 4-node interphase element.

Strain and stresses at the interphase can be separated into internal and contact components as follows:

$$\begin{array}{ll} \hat{\boldsymbol{\varepsilon}}^i = \left[\begin{array}{ccc} \hat{\varepsilon}_x & 0 & 0 \end{array} \right]^T & \hat{\boldsymbol{\sigma}}^i = \left[\begin{array}{ccc} \hat{\sigma}_x & 0 & 0 \end{array} \right]^T \\ \hat{\boldsymbol{\varepsilon}}^c = \left[\begin{array}{ccc} 0 & \hat{\varepsilon}_z & \hat{\gamma}_{xz} \end{array} \right]^T & \hat{\boldsymbol{\sigma}}^c = \left[\begin{array}{ccc} 0 & \hat{\sigma}_z & \hat{\tau}_{xz} \end{array} \right]^T \end{array} \tag{14}$$

In particular, strains can be related to nodal displacements using:

$$\begin{array}{l} \hat{\boldsymbol{\varepsilon}}^i = \mathbf{B}^i \mathbf{U} \\ \hat{\boldsymbol{\varepsilon}}^c = \mathbf{B}^c \mathbf{U} \end{array} \tag{15}$$

where $\mathbf{B}^i$ and $\mathbf{B}^c$ are two matrices containing the derivatives of the form functions. The total strains at the Gauss point is given by

$$\boldsymbol{\varepsilon} = \hat{\boldsymbol{\varepsilon}}^i + \hat{\boldsymbol{\varepsilon}}^c = \mathbf{B}\mathbf{U} \tag{16}$$

where $\mathbf{B} = \mathbf{B}^i + \mathbf{B}^c$.

Once the strains are known, the corresponding strains are obtained, in the elastic range, using the constitutive equations:

$$\hat{\boldsymbol{\sigma}} = \boldsymbol{E}\hat{\boldsymbol{\varepsilon}} \tag{17}$$

with $\mathbf{E} = \frac{E}{1-\nu^2} \left[\begin{array}{ccc} 1 & \nu & 0 \\ \nu & 1 & 0 \\ 0 & 0 & \frac{1-\nu}{2} \end{array} \right]$.

By applying the rotational operator $\boldsymbol{\theta}$ the $\mathbf{B}$ matrix can be rewritten with respect to the global reference system:

$$\mathbf{B}^* = \boldsymbol{B}\boldsymbol{\theta} \tag{18}$$

By using the classical procedure, minimizing the total potential energy, the nodal forces and the elastic stiffness matrix of the element are written as:

$$\mathbf{F} = \mathbf{K}\mathbf{U}; \quad \mathbf{K} = \int_V \mathbf{B}^{*T} \mathbf{E} \mathbf{B}^* dV. \tag{19}$$

4 INTERPHASE DAMAGE

The above interphase model can be characterized by a non-linear response if dissipation mechanisms such as damage or plasticity are included.

Following a thermodynamical approach, a local isotropic elastic-damage model can be created by adopting a free Helmholtz energy defined as

$$\Psi\left(\boldsymbol{\varepsilon}, \xi_d, \omega\right) = \frac{1}{2}\left(1-\omega\right)\boldsymbol{\varepsilon}^T \boldsymbol{E}\boldsymbol{\varepsilon} + \Psi_d\left(\xi_d\right) \tag{20}$$

where ω is the damage parameter calculated as the ratio between the damaged and the total area of a representative volume element of the material. It can assume values in the range $0 \leq \omega \leq 1$, with boundaries having the meaning of a pristine ($\omega = 0$) and a fully damaged material ($\omega = 1$) respectively. By evolution of ω the material's stiffness is continuously reduced. $\mathbf{E}$ is the material's undamaged elastic tensor, while $\boldsymbol{\varepsilon}$ is the strain tensor. Ψ_d represents a convex inelastic potential accounting for the evolution of the domain of linear elastic behaviour as a consequence of the activation of damage mechanisms, and it has been chosen equal to the expression furnished by [5]:

$$\Psi_d = h_d\left[\sum_{i=0}^{p-1}\frac{p!}{i!}\ln^i c + \ln^p c - \left(1-\xi_d\right)\sum_{i=0}^{p}\frac{p!}{i!}\ln^i\frac{c}{1-\xi_d}\right] \tag{21}$$

ξ_d has the rule of an internal variable used to describe the damage evolution. h_d, p and c are material's constants.

The state equations are obtained by derivation of Eq. 20 by ω, $\boldsymbol{\varepsilon}$ and ξ respectively:

$$\boldsymbol{\sigma} = \frac{\partial\Psi}{\partial\boldsymbol{\varepsilon}} \qquad \varsigma = -\frac{\partial\Psi}{\partial\omega} \qquad \chi_d = \frac{\partial\Psi}{\partial\xi_d} \tag{22}$$

Since the theorem of maximum dissipation is valid, the flow rules are derived looking for the maximum value of dissipation with respect to the static variables. The Lagrangian method is used to solve this problem. The Lagrangian is given by:

$$L = \boldsymbol{\sigma}^T\dot{\boldsymbol{\varepsilon}} - \dot{\Psi} - \dot{\lambda}_d\phi_d \tag{23}$$

where the dot means time derivative of the corresponding variable, λ_d is a lagrangian multiplier, and ϕ_d is a function that governs the activation and the evolution of damage. $\dot{\lambda}_d$ and ϕ_d have to respect the following loading/unloading complementarity conditions (Kuhn-Tucker relations):

$$\phi_d \leq 0; \quad \dot{\lambda}_d \geq 0; \quad \phi_d\dot{\lambda}_d = 0 \tag{24}$$

An explicit expression of ς is

$$\varsigma = \frac{1}{2}\boldsymbol{\varepsilon}^T\boldsymbol{E}\boldsymbol{\varepsilon}. \tag{25}$$

On the other side, $\boldsymbol{\varepsilon}$ can be rewritten as the sum of two different vectors, if we would separate the contribution of positive or negative values of longitudinal strains. As such:

$$\boldsymbol{\varepsilon} = \boldsymbol{\varepsilon}^+ + \boldsymbol{\varepsilon}^- = \begin{bmatrix} \langle\varepsilon_x\rangle \\ \langle\varepsilon_z\rangle \\ \gamma_{xz} \end{bmatrix} - \begin{bmatrix} \langle-\varepsilon_x\rangle \\ \langle-\varepsilon_z\rangle \\ 0 \end{bmatrix} \tag{26}$$

where $\langle \bullet \rangle$ indicates the McAuley brackets defined as $\langle \bullet \rangle = \frac{\bullet + |\bullet|}{2}$.

By substituting Eq. 26 into 25 and by simple calculation it is obtained that:

$$\varsigma = \varsigma^+ + \varsigma^- \tag{27}$$

with

$$\varsigma^+ = \frac{E}{2\left(1-\nu^2\right)}\left[\langle \varepsilon_x \rangle^2 + \langle \varepsilon_z \rangle^2 + 2\nu \langle \varepsilon_x \rangle \langle \varepsilon_z \rangle + \frac{1-\nu}{2}\gamma_{xz}^2\right] \tag{28}$$

$$\varsigma^- = \frac{E}{2\left(1-\nu^2\right)}\left[\langle -\varepsilon_x \rangle^2 + \langle -\varepsilon_z \rangle^2 + 2\nu \langle -\varepsilon_x \rangle \langle -\varepsilon_z \rangle - 2\nu \langle \varepsilon_x \rangle \langle -\varepsilon_z \rangle - 2\nu \langle -\varepsilon_x \rangle \langle \varepsilon_z \rangle\right]. \tag{29}$$

It can be observed from Eq. 28 that only positive parameters' values are included into ς^+, while negative or mixed (positive and negative strains) contributions are relegated into ς^-.

By using the last definition of ς, the damage activation function is written as:

$$\phi_d = \varsigma^+ - \chi_d \leq 0 \tag{30}$$

that allows to write the flow rules of the kinematic quantities by using the Lagrangian method:

$$\dot{\omega} = \dot{\lambda}_d \qquad \dot{\xi}_d = \dot{\lambda}_d \tag{31}$$

5 INTERPHASE ELEMENT PERFORMANCE

In order to validate the model, some examples were carried out by using the FEAP finite element program. Different goals were looked for. First, it was important to show the behaviours of the elasto-damaging model by means of simple examples such as a single-layer mortar masonry specimen subjected to compressive loads. Second, it was opportune to highlight the improvements given by the enriching terms in the interphase with respect to an interface model. Third, it was due to show the applicability of the interphase elements at the mesoscopic level inside a finite element model, and results compared with experimental data.

The first example regarded a system made up of two blocks interposed by a mortar layer. The system was subjected to a compressive monotonic load. In Fig. 3a it is shown the finite element mesh of bricks and mortar and the Gauss points in the interphase elements. Tests were made using different ratios of elastic moduli for bricks and mortar. Fig. 3b shows the applied force-vertical displacement diagram for the two points A and B of Fig. 3a for an elastic modulus of the interphase higher than the elastic modulus of bricks ($E_i = 10E_b$).

Due to the different elastic modulus the interphase is subjected to a tensile stress while the bricks are constrained by the mortar and then subjected to a compressive stress. After an initial elastic behaviour the tensile stress in the mortar leads to the opening of a fracture starting from the middle of the mortar joint, step 83. Further increase of the load causes a different behaviour in terms of vertical diplacement response between central and lateral part of the joint as shown in Fig. 3b. In fact the damage increases in the central part, step 120, leading to a snap back phenomenon for central node A till the complete fracture of the mortar joint, step 170.

In Fig. 4 are represented the response in terms of internal quantities ε_x and σ_x (Fig. 4a, b) and in terms of contact stress σ_z (Fig. 4c) and damage parameter ω (Fig. 4d).

As expected for the first steps deformation and stress are almost constant along the joint, step 41. Due to the increase of internal stress σ_x damage starts to develope, step 83, leading to a redistribution

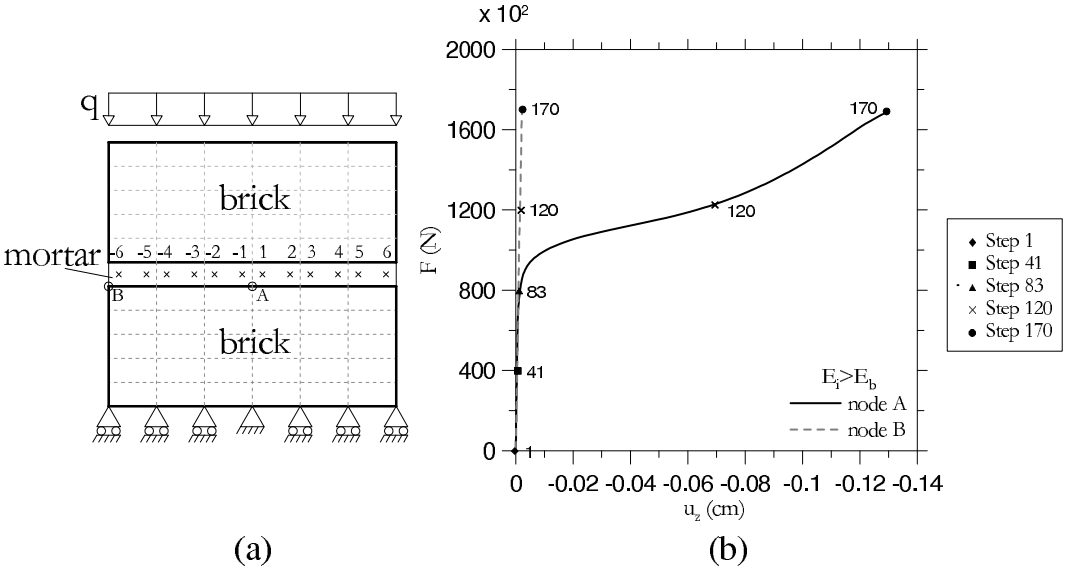

Figure 3: (a) Finite element mesh for compressive test; (b) load-displacement curve at the two nodes A and B ($E_i = 10E_b$).

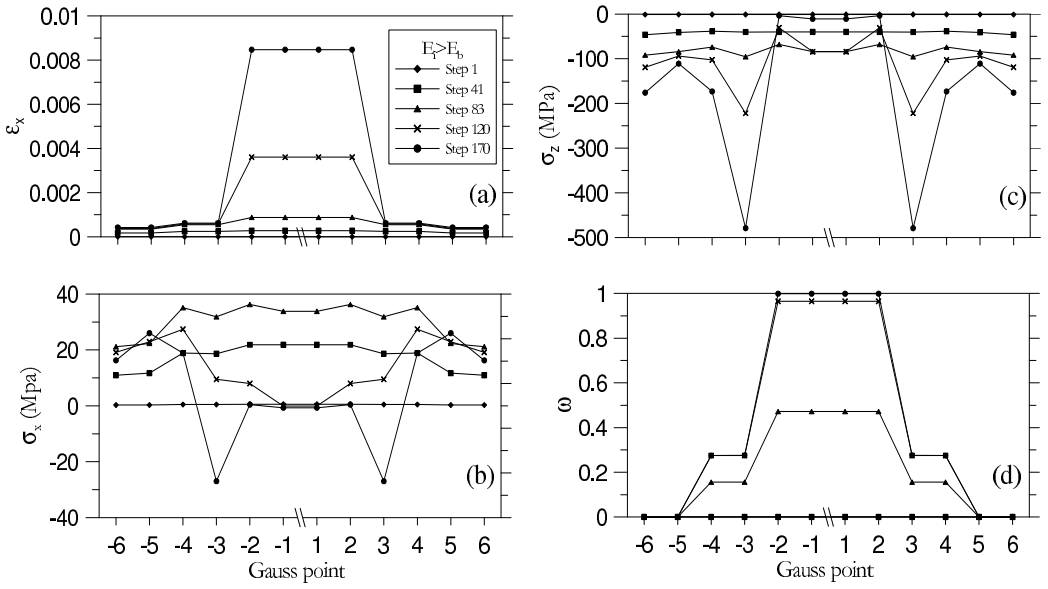

Figure 4: $E_i = 10E_b$: (a) internal deformation ε_x, (b) internal stress σ_x, (c) contact stress σ_z, (d) damage parameter ω distributions in corrispondence of the Gauss points.

of stresses, both internal and constant ones, from central part to undamaged lateral one, step 120. The process follows till the complete fracture of the mortar joint as shown by the values of stresses and damage parameter, step 170.

The same test was developed with an inverse ratio between elastic modulus of bricks and mortar joint, ($E_i = E_b/10$). Fig. 5 shows the force-displacement curve for this case. It is clear as this time is node B that went up after step 200. The curve is linear until the onset of the fracture that was expected to start at the extreme points. The jump in the diagram is due to a sudden rupture of different Gauss points. Fig. 6 confirms the results in Fig. 5. The damage parameter started to increase at the external Gauss points with a consequent reduction of the stress together with an increase of vertical displacements at these points. Parameters used to run this first example are: $E_b = 10000\ N/mm^2$; $\nu_b = \nu_i = 0.15$; $\varsigma_0 = 0.01\ N/mm^2$; $p = 3$; $c = 3$; $E_i = 1000\ N/mm^2$ (Figs. 3 and 4); $E_i = 100000\ N/mm^2$ (Figs. 5 and 6).

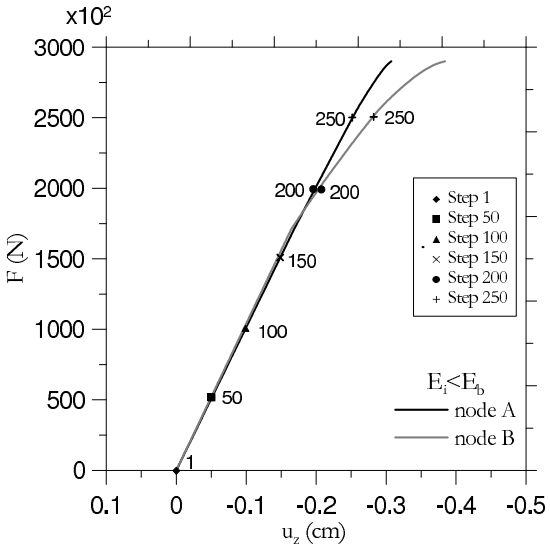

Figure 5: $E_i = E_b/10$: load-displacement curve at the two nodes A and B.

6 NUMERICAL APPLICATION TO PULL-OUT TESTS

In the second example interphase elasto-damaging elements were used to model the resin in chemically bonded anchors. A specimen ready to be tested and the relative mesh are shown in Fig. 7. Experimental material properties were determined following [6]-[8].

Four different test results are here reported. The first three tests were performed on an anchorage length of $152.4\ mm$ ($6\ in$), the last one on an anchorage length of $101.6\ mm$ ($4\ in$).

While in the cast-in-place anchors the load is transferred into the concrete at the anchor head, in the case of adhesive anchors the load is transferred from the steel through the adhesive layer along the entire bonded surface. The bond at the interface consists of three mechanisms: adhesion, friction and mechanical interlock.

When rebars are chemically bonded, the higher tensile limit stress leads to different possible types of failure modes, depending on the boundary and anchoring conditions. The typical failure

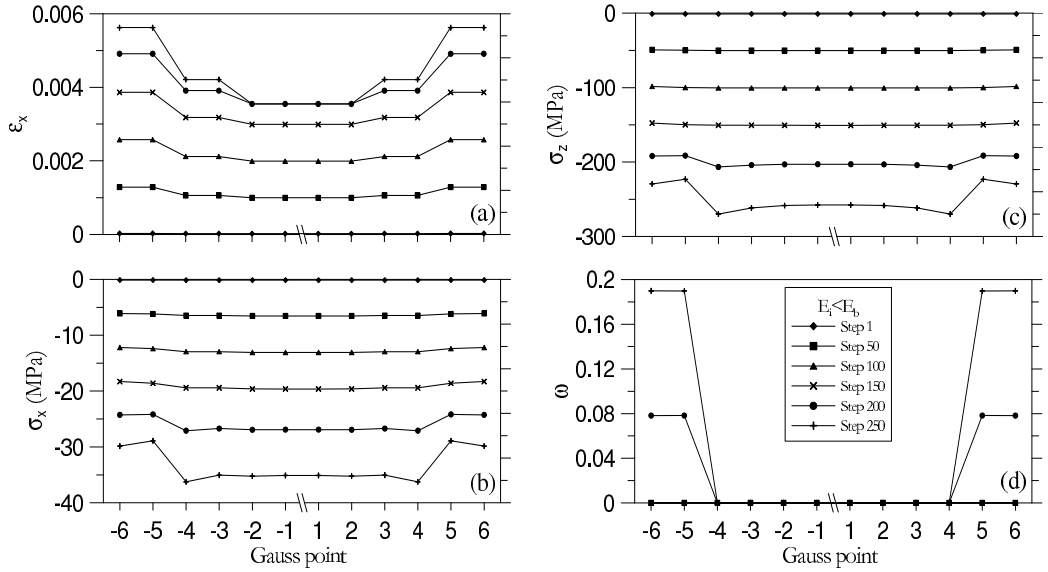

Figure 6: $E_i = E_b/10$: (a) internal deformation ε_x, (b) internal stress σ_x, (c) contact stress σ_z, (d) damage parameter ω distributions in corrispondence of the Gauss points.

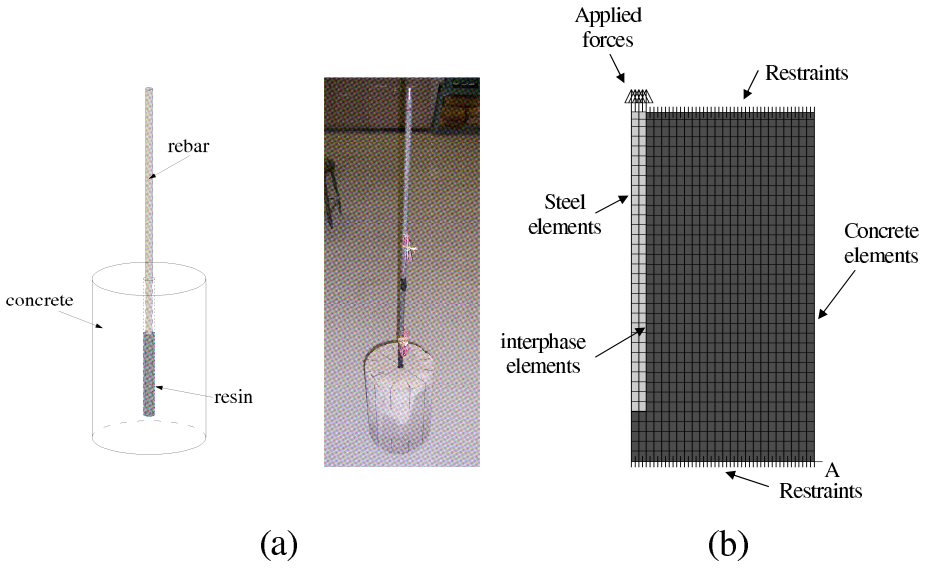

Figure 7: (a) A specimen for the pullout test; (b) Finite element mesh.

modes are showed in Fig. 8 and can be classified as ([1], [9]):

1) Anchor steel failure characterized by yielding or fracture of the steel;

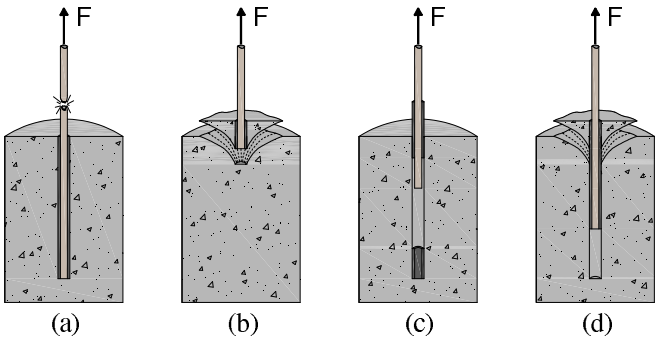

Figure 8: Failure modes during a pullout test for unconfined concrete: (a) steel failure; (b) concrete cone failure; (c) bond failure; (d) combined cone-bond failure.

2) Concrete cone failure occurring when the embedment depth is less than $50\ mm$ and the concrete is unconfined;

3) Bond failure at the bar/resin or resin/concrete interface;

4) Combined cone-bond failure usually in unconfined concrete and embedment depth greater than $50 - 100\ mm$.

Several variables influence the tensile pullout strength of bonded rebars, namely bonding agent, concrete, steel, surface roughness, temperature, loading gradient ([1], [9]).

An axisymmetric model has been implemented in the finite element program FEAP to simulate the pullout tests. Only three materials are needed for the analysis: steel, interphase and concrete.

Bi-dimensional 4-noded rectangular shape elements were used in FEAP to model the solid elements. The concrete has an elastic modulus of $E = 21197\ MPa$ and a Poisson's ratio equal to $\nu = 0.16$. The rebar was assumed smooth and elastoplastic, with elastic tensile limit equal to $418\ MPa$ and plastic hardening equal to $20\ MPa$, $E = 210000\ MPa$ and $\nu = 0.30$. Two Gauss points were selected as integration points for each interphase element. The parameters used for the interphase elements were chosen on the base of the experimental results.

The boundary condition included restraint of vertical displacements on top of the concrete. This restraint together with the appropriate bond length allows for shear pullout failure only and avoids the concrete cone failure. Other restraints were imposed to the vertical displacements at the bottom of the cylinder, and radial and vertical displacements of the node A indicated in Fig. 7b.

The numerical simulations were carried out using the *arclength solution* ([3]-[4]).

Fig. 9 reports the experimental results together with the numerical ones. The rebars used in Tests 1 and 2 reached the yielding. At the end of the tests, as the ribs were clearly visible, it can be deduced that debonding occurred at the rebar/resin interface due to shear pullout failure. Every experimental curve is characterized by an initial nonlinear behavior due to the start-up and the adjustment of the grips of the loading machine, followed by the linear behavior typical of the linear elastic range. The onset of debond occurred around $85\ kN$. The tests were conducted until complete debond was observed. The area where damage onset and propagation occurred is characterized by the softening branch shown in Fig. 9. The structural response at softening is affected by the amount of damage occurring at the interface. In addition as the rebar pulls out, the contact surface between the resin/rebar and the resin/concrete interface decreases. Such a decrease reduces the friction force between the ribs and the surrounding material affecting the force-displacement response of the struc-

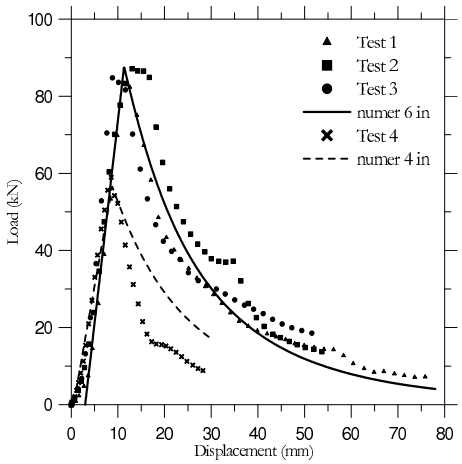

Figure 9: Experimental and numerical load-displacement curves during the pullout tests.

ture at softening.

In Tests 1 and 3, the transition from the linear elastic to the softening regime was rapid. In Tests 2, however, a slight variation of the linear slope was visible at about $70\ kN$. This behavior was probably due to damage onset localized in a weak zone of the interface that failed prior to the occurrence of the main debonding.

The load-displacement results of Tests 1-3 were used to calibrate the parameters of the interphase model, that are: $\varsigma_0 = 4.5\ N/mm^2$; $p = 5$; $c = 40$; $E_i = 7.5\ N/mm^2$; $\nu = 0.25$. A good agreement was found between the experimental and numerical results.

In the same figure the result for Test 4 was also reported together with the numerical simulation for a bonded length equal to $101.6\ mm$ ($4\ in$). Obviously, the same interphase parameters were used. In this case the numerical model overestimated the softening branch, probably because a non uniform distribution of the resin along the bonded length, even if the general trend was recognized.

7 CONCLUSIONS

In this paper a damage interphase model has been presented and its features discussed. The model has been implemented as a new finite element. The performance of the interphase element has been validated by means of a single-layer mortar masonry specimen subjected to compressive loads. Finally, an axisymmetric model has been used to compare numerical and experimental results of pull-out tests on rebars embedded into concrete.

ACKNOWLEDGEMENTS.

The authors acknowledge the financial support given by the Italian Ministry of Education University and Research (MIUR) under the PRIN07 Project 2007YZ3B24, ”Multi-scale problems with complex interactions in Structural Engineering”.

References

[1] Cook, R.A., "Behavior of chemically bonded anchors," *ASCE Journal of Structural Engrg.*, **119(1)**, 2744-2762 (1993).

[2] Giambanco, G., Mróz, Z., "The interphase model for the analysis of joint in rock masses and masonry structures," *Meccanica*, **36**, 111-130 (2001).

[3] Taylor, R. L., "FEAP - - A Finite Element Analysis Program," *Version 7.5 User Manual*, (2005a).

[4] Taylor, R. L., "FEAP - - A Finite Element Analysis Program," *Version 7.5 Programmer Manual*, (2005b).

[5] Comi, C., Perego, U., "Criteria for mesh refinement in nonlocal damage finite element analyses," *European Journal of Mechanics A/Solids*, **23(1)**, 615-632 (2004).

[6] ASTM C469-94, "Standard test method for static modulus of elasticity and Poisson's ratio of concrete in compression," 248-251 (1994).

[7] ASTM C39/C 39M-01, "Standard test method for compressive strength of cylindrical concrete specimens," 18-22 (2001).

[8] ASTM C617-98, "Standard practise for capping cylindrical concrete specimens," 305-309 (1998).

[9] Sakla, S.S.S., Ashour, A.F., "Prediction of tensile capacity of single adhesive anchors using neural networks," *Computers and Structures*, **83(1)**, 1792-1803 (2005).

[10] Castro, P.F., "Influence of coatings on bar-concrete bond," *ASCE Journal of Materials in Civil Engrg*, **8(4)**, 212-214 (1996).

[11] Gambarova, P.G., Rosati, G.P., Schumm, C., "An elasto-cohesive model for steel-concrete bond," *Fracture and Damage in Quasi brittle Structures*, 557-566 (1994).

[12] Lemaitre, J., Chaboche, J. L. , *Mechanichs of solids materials*, University Press, Cambridge (1990).

[13] Maugin, G.A., *The thermomechanics of plasticity and fracture*, University Press, Cambridge (1992).

[14] McVay, M., Cook, R.A., Krishnamurthy, K., "Pullout simulation of post-installed chemically bonded anchors," *Journal of Structural Engrg*, **122(1)**, 1016-1024 (1996).